Convergent evolution of a blood-red nectar pigment in vertebrate-pollinated flowers

Rahul Roy[a], Nickolas Moreno[b], Stephen A. Brockman[c], Adam Kostanecki[a], Amod Zambre[d], Catherine Holl[a], Erik M. Solhaug[a], Anzu Minami[a], Emilie C. Snell-Rood[d], Marshall Hampton[e], Mark A. Bee[d], Ylenia Chiari[b], Adrian D. Hegeman[a,c,1], and Clay J. Carter[a,1]

[a]Department of Plant and Microbial Biology, University of Minnesota, St. Paul, MN 55108; [b]Department of Biology, George Mason University, Fairfax, VA 22030; [c]Department of Horticultural Science, University of Minnesota, St. Paul, MN 55108; [d]Department of Ecology, Evolution, and Behavior, University of Minnesota, St. Paul, MN 55108; and [e]Department of Mathematics and Statistics, University of Minnesota Duluth, Duluth, MN 55812

Edited by Natasha Raikhel, Department for Botany and Plant Science, University of California, Riverside, Center for Plant Cell Biology, Riverside, CA; received August 5, 2021; accepted December 10, 2021

Nearly 90% of flowering plants depend on animals for reproduction. One of the main rewards plants offer to pollinators for visitation is nectar. *Nesocodon mauritianus* (Campanulaceae) produces a blood-red nectar that has been proposed to serve as a visual attractant for pollinator visitation. Here, we show that the nectar's red color is derived from a previously undescribed alkaloid termed nesocodin. The first nectar produced is acidic and pale yellow in color, but slowly becomes alkaline before taking on its characteristic red color. Three enzymes secreted into the nectar are either necessary or sufficient for pigment production, including a carbonic anhydrase that increases nectar pH, an aryl-alcohol oxidase that produces a pigment precursor, and a ferritin-like catalase that protects the pigment from degradation by hydrogen peroxide. Our findings demonstrate how these three enzymatic activities allow for the condensation of sinapaldehyde and proline to form a pigment with a stable imine bond. We subsequently verified that synthetic nesocodin is indeed attractive to *Phelsuma* geckos, the most likely pollinators of *Nesocodon*. We also identify nesocodin in the red nectar of the distantly related and hummingbird-visited *Jaltomata herrerae* and provide molecular evidence for convergent evolution of this trait. This work cumulatively identifies a convergently evolved trait in two vertebrate-pollinated species, suggesting that the red pigment is selectively favored and that only a limited number of compounds are likely to underlie this type of adaptation.

nectar | nectaries | gecko | *Nesocodon* | *Jaltomata*

Pigments mediate essential physiological and ecological functions throughout all domains of life, from roles in ultraviolet protection in both eukaryotes and prokaryotes (1) to light-regulated development and establishment of circadian rhythms (2) to visual signaling and mate choice in animals (3). Among plants, flower color is often crucial in pollinator attraction (4). Plant–pollinator interactions have driven at least a portion of the massive species radiation observed in the angiosperms, leading not only to extremely diverse floral size and morphology (5) but also to the accompanying chemistries behind attractants (color and scent) and rewards (nectar and pollen) (e.g., Refs. 6–9). Although rare, one floral trait that has evolved multiple times is colored nectar (10), which has been suggested to serve as an "honest" visual cue of a reward to prospective pollinators (10, 11).

Approximately 70 plant species are known to produce colored nectars (10), with one charismatic example being the blood-red nectar of *Nesocodon mauritianus* (12), which reportedly gets its color from 3′,5′-dihydroxy-4′-methoxyaurone (12). Several Mauritian plants with colored nectars, including *Nesocodon*, are known or suspected to be pollinated by day geckos (13). A previous field study reported that two Mauritian species with colored nectars are visited and pollinated by day geckos (*Phelsuma* spp.) and that artificial nectars containing commercially available red food coloring are attractive to these geckos (13). Beyond *Nesocodon*, one report suggested that the purple nectar of *Leucosceptrum canum* contains 5-hydroxyflavylium to attract bird pollinators (14), whereas a conflicting report claimed the pigment to be a benzoquinone derivative (15). No other reports exist on the putative identities, syntheses, or function(s) of colored nectars. This study reports an investigation into the biochemical nature and biological function of *Nesocodon*'s red-pigmented nectar within a phylogenetic and evolutionary framework to address our gap in knowledge of colored nectars.

Nectar Color with Respect to Floral Phenology

Nesocodon nectar is well known to have a deep red color, but a phenological examination of nectar production has not been reported. Toward this end, we found that newly opened *Nesocodon* flowers (0 h) actually have a yellow nectar (Fig. 1 *A* and *B*; *SI Appendix*, Fig. S1), which gradually turns orange (+8 h; Fig. 1*E*) and then red (+24 h; Fig. 1 *C*–*E*). The progression from yellow to orange to red positively corresponds to nectar

Significance

Beyond sugars, many types of nectar solutes play important ecological roles; however, the molecular basis for the diversity of nectar composition across species is less explored. One rare trait among flowering plants is the production of colored nectar, which may function to attract and guide prospective pollinators. Our findings indicate convergent evolution of a red-colored nectar has occurred across two distantly related plant species. Behavioral data show that the red pigment attracts diurnal geckos, the likely pollinator of one of these plants. These findings join a growing list of examples of distinct biochemical and molecular mechanisms underlying evolutionary convergence and provide a fascinating system for testing how interactions across species drive the evolution of novel pigments in an understudied context.

Author contributions: R.R., N.M., S.A.B., A.K., A.Z., C.H., E.M.S., A.M., E.C.S.-R., M.H., M.A.B., Y.C., A.D.H., and C.J.C. designed research; R.R., N.M., S.A.B., A.K., A.Z., C.H., E.M.S., A.M., M.H., Y.C., A.D.H., and C.J.C. performed research; R.R., N.M., A.K., A.Z., A.M., E.C.S.-R., M.H., M.A.B., Y.C., A.D.H., and C.J.C. analyzed data; and A.Z., A.M., E.C.S.-R., M.H., M.A.B., Y.C., A.D.H., and C.J.C. wrote the paper.

Competing interest statement: A.D.H. and C.J.C. are named on a patent application (US2020/0474) by the University of Minnesota on the synthesis of the nesocodin pigment and associated non-natural derivatives.

This article is a PNAS Direct Submission.

See online for related content such as Commentaries.

[1]To whom correspondence may be addressed. Email: hegem007@umn.edu or cjcarter@umn.edu.

This article contains supporting information online at http://www.pnas.org/lookup/suppl/doi:10.1073/pnas.2114420119/-/DCSupplemental.

Published January 24, 2022.

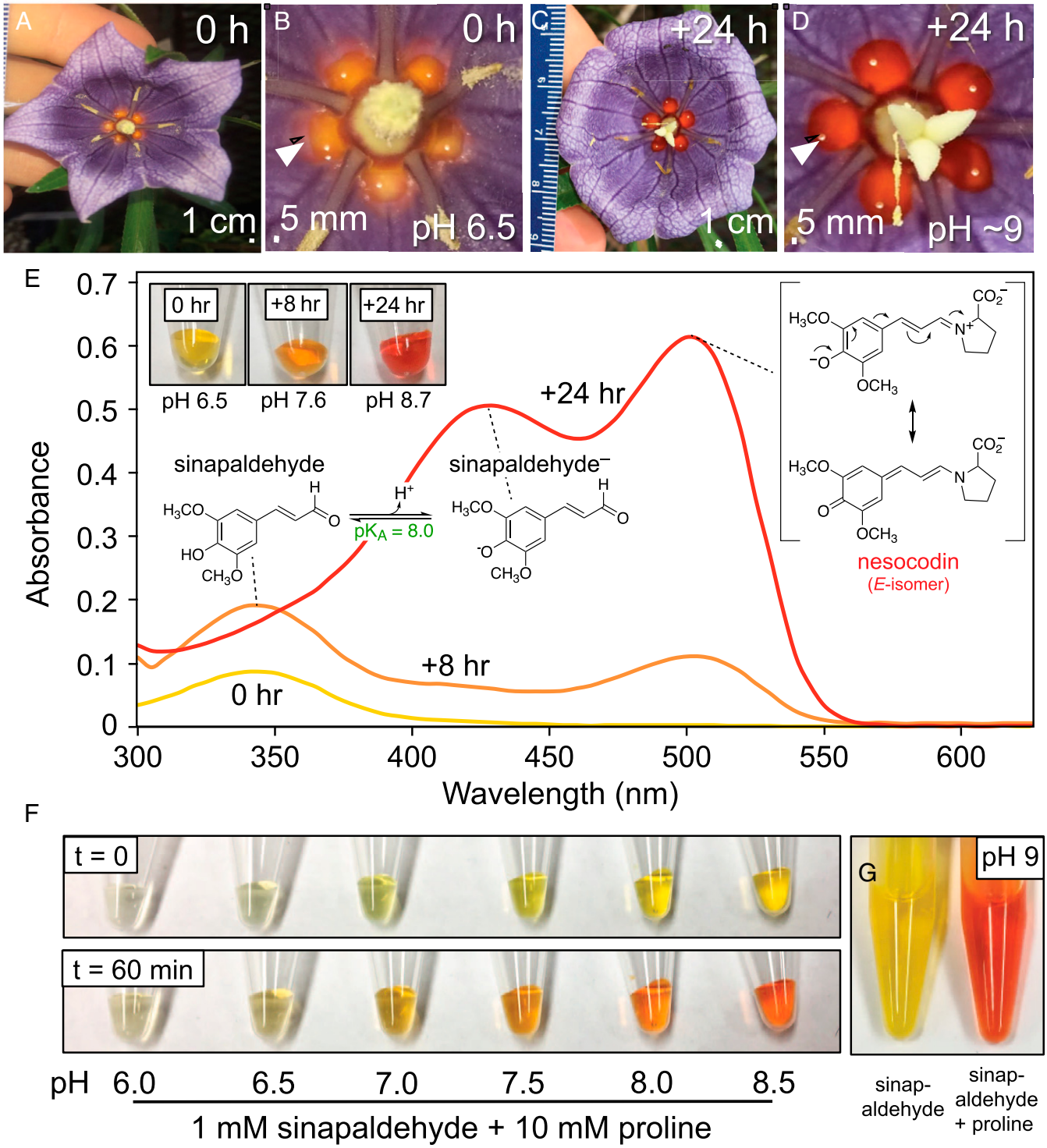

Fig. 1. The color and pH of *N. mauritianus* nectar change over time. (*A* and *B*) Newly opened flower (0 h); *B* is a close-up of *A* showing the color of five distinct nectar droplets (arrowhead). (*C* and *D*) Flower ~24 h after opening; *D* is a close-up of *C*. (*E*) UV/visible absorbance spectra of nectars collected at 0 h (yellow), +8 h (orange), and +24 h (red) after dilution at 1:50 in deionized H_2O. Images of each undiluted nectar and pH are noted in the *Inset*. Structures of the pigments contributing to the absorbance peaks were initially identified by LC-MS (*SI Appendix*, Figs. S3, S4, and S9) and confirmed by multiple approaches (*SI Appendix*, Figs. S7, S8, S10–S14). (*F*) pH-dependent formation of colored products derived from 1 mM sinapaldehyde and 10 mM proline in 25 mM buffers of varying pH, including 6.0 (MES), 6.5 (MES), 7.0 (HEPES), 7.5 (HEPES), 8.0 (HEPES), and 8.5 (Tricine). (*G*) Color of 1 mM sinapaldehyde in 50 mM $Na(H)CO_3$ (pH 9.0), with and without 10 mM L-proline after a 30-min incubation at 21 °C.

alkalinization (Fig. 1*E*). Artificial alkalinization of yellow nectar (0 h) shifts the UV/visible absorbance maximum (λ_{MAX}) from 343 nm to 430 nm but does not yield a red color (*SI Appendix*, Fig. S2*A*). Conversely, stepwise acidification of red nectar (+24 h) yields a yellow color by proportionally decreasing the major absorbance peak at 505 nm, with a concomitant increase in a

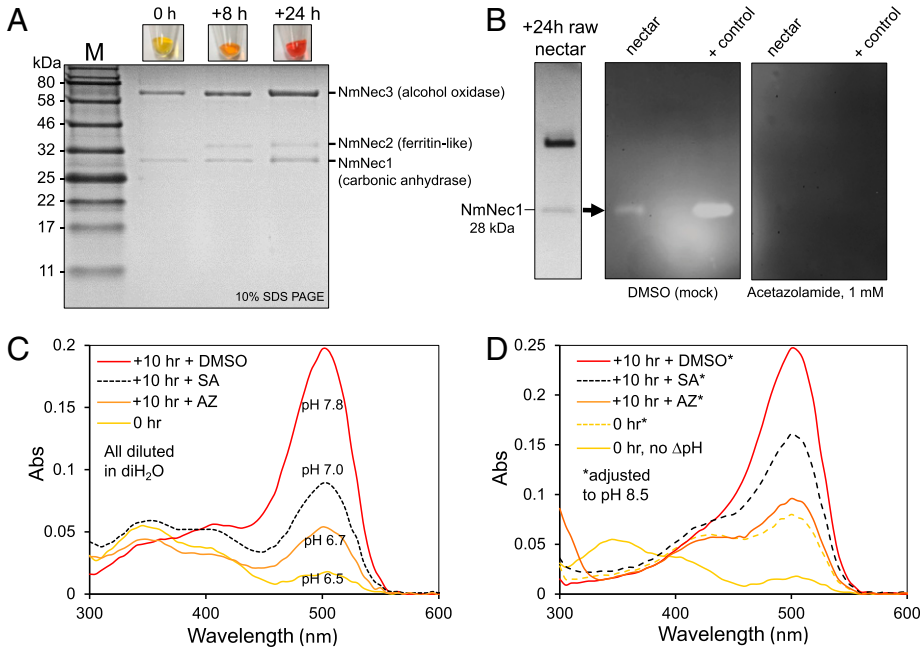

Fig. 2. A carbonic anhydrase is responsible for nectar alkalinization. (*A*) SDS-PAGE analysis of 0 h, +8 h, and +24 h nectars (18 μL each; see *SI Appendix*, Fig. S17 for protein identification). (*B*) In-gel carbonic anhydrase assay of 18 μL of +24 h nectar and a positive control without (*Left*) and with (*Right*) 1 mM acetazolamide added. (*C*) UV/visible absorbance (Abs) spectra and pH of nectar droplets treated in situ with carbonic anhydrase inhibitors. The carbonic anhydrase inhibitors sulfanilamide (SA) or acetazolamide (AZ) were added to separate 0-h nectar droplets in the same flower to a final concentration of 1 mM; a mock treatment containing an equal volume of 10% DMSO was included; one untreated nectar droplet was collected at 0 h and stored at 4 °C in the dark; and the treated nectar droplets were subsequently collected at +10 h, measured for pH, diluted 1:50 in H_2O, and evaluated by UV-Vis spectrophotometry. (*D*) Absorbance spectra of the same nectars from panel *C* after diluting 1:50 with 50 mM Tricine (pH 8.5). Additional representative results from individual treated flowers are shown in *SI Appendix*, Fig. S20.

peak present in the yellow (0 h) nectar at ~343 nm and a separate peak at 403 nm (*SI Appendix*, Fig. S2*B*). The red color rapidly returns with realkalinization of the artificially acidified +24 h nectar with a λ_{MAX} of 505 nm. These results cumulatively indicate that the compound responsible for the nectar's red color has a λ_{MAX} of 505 nm under alkaline conditions, which shifts to 403 nm upon acidification.

Pigment Identification

Using these pH-dependent absorbance maxima as key diagnostics, liquid chromatography-mass spectrometry (LC-MS) and MS/MS analyses of yellow (0 h) and red (+24 h) nectar under acidic mobile conditions identified an eluting peak with an *m/z* of 209.0807 (± 0.0004) and λ_{MAX} of ~343 nm (*SI Appendix*, Fig. S3, i.e., corresponds to the major absorption peak in 0 h nectar; *SI Appendix*, Fig. S2). This compound was identified as sinapaldehyde [(E)-3,5-dimethoxy-4-hydroxycinnamaldehyde]) by fragmentation analysis and comparison of chromatographic and UV/visible spectroscopic properties to a commercially obtained standard (*SI Appendix*, Figs. S3 and S4). Sinapaldehyde is a major component of lignin in the secondary cell walls of plant cells (16) but has not yet been reported as a nectar component.

LC-MS/MS analysis of red nectar (+24 h) also identified another major peak with an *m/z* of 306.1333 (± 0.0006) and λ_{MAX} of 403 nm matching that of acidified red nectar (*SI Appendix*, Figs. S2*B* and S3). Similarities in MS/MS fragmentation suggested that the red pigment results from conjugation of sinapaldehyde with another nectar constituent. The exact mass difference between the conjugate and sinapaldehyde plus the mass of water of hydrolysis is 115.0632, which matches the elemental composition of the amino acid proline ($C_5H_9NO_2$). Like the nectars of several distantly related species, including those of tobacco and soybean (17), we found that free proline accumulates to high levels in *Nesocodon* nectar (up to ~60 mM; e.g., *SI Appendix*, Fig. S6). We postulated that the red pigment is an imine conjugate of proline and sinapaldehyde, the formation of which depends on the deprotonation of proline such that the equilibrium shifts toward the formation of the red conjugate with increasing pH (*SI Appendix*, Fig. S5*A*). Indeed, aqueous mixtures of sinapaldehyde and proline produced a pH-dependent, red-colored compound in vitro, hereafter referred to as "nesocodin" (Fig. 1 *F–G*; *SI Appendix*, Fig. S5*B*). The reduction of nesocodin using sodium borohydride ($NaBH_4$) or sodium borodeuteride ($NaBD_4$) resulted in both a loss of color and accumulation of the expected products of imine reduction (*SI Appendix*, Fig. S7). The spectroscopic, spectrometric, and chromatographic properties of synthetic nesocodin were identical to those of the natural pigment (*SI Appendix*, Figs. S8 and S9). Anhydrous synthetic reaction conditions were then devised and provided quantitative conversion of L-proline and sinapaldehyde to nesocodin, which was structurally characterized by NMR (*SI Appendix*, Figs. S10–S14) and found to form as a mixture of *E*- and *Z*-isomers (~2:1). Similar separation of these isomers by ultra-high– performance liquid chromatography analysis in both synthetic and nectar-derived nesocodin (*SI Appendix*, Fig. S15) suggests that imine conjugation in vivo is nonenzymatic.

The pH dependence of nesocodin production led to several conclusions: 1) nectar alkalinization is essential for proline deprotonation to shift the equilibrium toward nesocodin formation (*SI Appendix*, Fig. S5); 2) the absorbance spectra of both nesocodin and sinapaldehyde display bathochromic shifts as these compounds are deprotonated (pK_As of 6.5 and 8.0, respectively; *SI Appendix*, Figs. S5 and S16), which is sufficient for the blood-red coloration of mature nectar; and 3) nesocodin is likely stabilized by resonance delocalization (Fig. 1*E*) upon deprotonation, a phenomenon expected to positively affect its

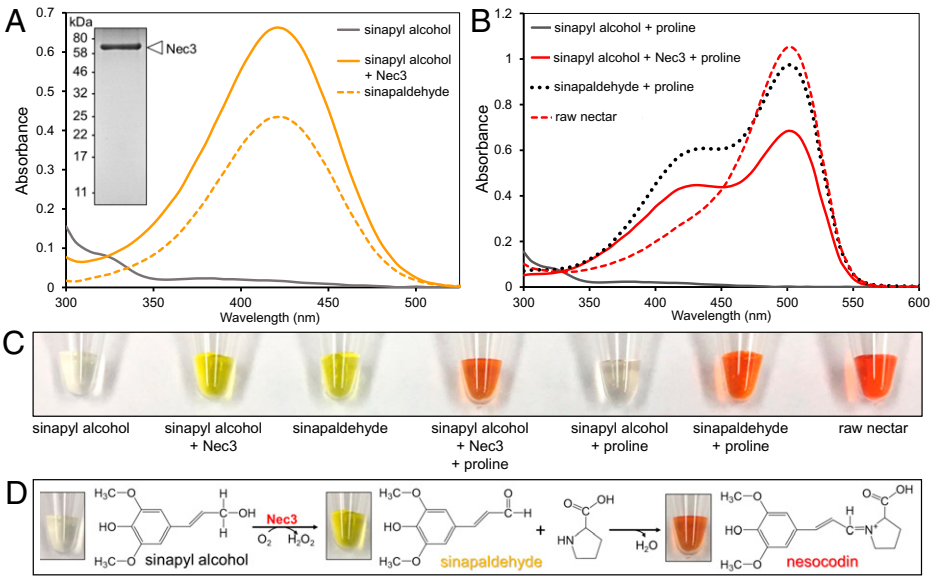

Fig. 3. NmNec3 can oxidize sinapyl alcohol into sinapaldehyde to serve as a precursor to nesocodin. (*A*) Purified NmNec3 (*Inset*) has sinapyl alcohol oxidase activity and can produce sinapaldehyde. The absorbance spectrum shown by the solid yellow line is the result of a reaction mix containing 1 mM sinapyl alcohol and 0.1 μg/mL NmNec3 in 50 mM $Na(H)CO_3$ (pH 9.0). Negative controls with sinapyl alcohol but no NmNec3 did not yield any sinapaldehyde (gray line); a 0.5 mM sinapaldehyde standard in 50 mM $Na(H)CO_3$ (pH 9.0) was used as a reference (dotted yellow line). (*B*) The same reactions as in *A* (with NmNec3), but also containing 10 mM proline produced a red-colored product (solid red line) consistent with both synthetic nesocodin (black dotted line; 1 mM sinapaldehyde plus 10 mM proline) and raw nectar (red dashed line; diluted 1:20). (*C*) Representative images showing the colors of the products of panels *A* and *B*. (*D*) Reaction sequence between sinapyl alcohol, NmNec3, and proline to yield nesocodin.

accumulation in aqueous systems (18). It is also clear that the nectar's red color is not derived from 3′,5′-dihydroxy-4′-methoxyaurone, as previously reported (12).

Pigment Biosynthesis

Since nesocodin formation and stability requires alkaline conditions, we next sought factors that increase nectar pH. Sodium dodecyl sulfatepolyacrylamide gel electrophoresis (SDS-PAGE) analysis revealed the presence of three major nectar proteins at ~28, 30, and 65 kDa, which we termed NmNec1, NmNec2, and NmNec3 in order of increasing molecular weight. Subsequent in-gel trypsinization and proteomic analyses (facilitated by a translated nectary transcriptome [National Center for Biotechnology Information Sequence Read Archive (NCBI SRA) GSE149898]) identified these three major nectar proteins as a putative α-type carbonic anhydrase (NmNec1, 28 kDa), a desiccation-related protein with a ferritin-like domain (NmNec2, 30 kDa), and a mandelonitrile lyase-like protein in the glucose-methanol-choline (GMC) oxidoreductase protein superfamily (NmNec3, 65 kDa) (Fig. 2*A*; *SI Appendix*, Figs. S17 and S18). All three of these nectar proteins contain predicted N-terminal signal peptides for secretion from the cell (*SI Appendix*, Fig. S17 *A–C*). Moreover, no tryptic peptides from the proteomic analyses correspond to the predicted signal peptides, which suggests that they are cleaved from the final proteins as expected. *NmNec1* and *NmNec3* display enriched expression in nectaries, whereas *NmNec2* appears to be ubiquitously expressed in flowers (*SI Appendix*, Fig. S17*D*).

NmNec1 Is a Carbonic Anhydrase that Increases Nectar pH. Carbonic anhydrases help regulate both extracellular and cytosolic pH in animals, including cases of extreme alkalinization (19); thus, we predicted NmNec1 plays a role in increasing nectar pH. NmNec1 is an alpha-type carbonic anhydrase (*SI Appendix*, Fig. S18) and has carbonic anhydrase activity that is inhibitable with either of the known carbonic anhydrase inhibitors sulfanilamide or acetazolamide in vitro (e.g., Fig. 2*B* and *SI Appendix*, Fig. S19*A*). Conversely, adding bicarbonate to 0 h nectar increases nectar pH in vitro, whereas buffers of equivalent molarity and pH does not (*SI Appendix*, Fig. S19*B*). Similarly, removal of yellow nectar (0 h) from flowers prevented further alkalinization (*SI Appendix*, Fig. S19*C*), suggesting that the nectary supplies nectar with bicarbonate. The nectar droplets on *Nesocodon* flowers remain physically separated until a few days after opening (Fig. 1*A*). We took advantage of this characteristic by adding carbonic anhydrase inhibitors directly to individual nectar droplets in situ. Addition of sulfanilamide, acetazolamide, or 6-ethoxy-2-benzothiazolesulfonamide decreased both nectar alkalinization and absorbance at 505 nm (Fig. 2*C*; *SI Appendix*, Fig. S20). The same treated nectar droplets showed less red pigment formation relative to control droplets when adjusted to alkaline pH (Fig. 2*D*), confirming that little nesocodin is produced under acidic-to-neutral conditions (*SI Appendix*, Fig. S5*B*).

NmNec3 Synthesizes Sinapaldehyde from Sinapyl Alcohol. Given the acidic pH of most intracellular compartments, it is unlikely that nesocodin could be made intracellularly and then secreted, so we next questioned whether other nectar proteins mediate pigment formation. NmNec3 belongs to the GMC flavoenzyme oxidoreductase family (*SI Appendix*, Fig. S21), which includes mandelonitrile lyases and several known examples of alcohol oxidases (20). Purified NmNec3 (Fig. 3*A*) was verified as a flavoprotein (*SI Appendix*, Fig. S22*A*) with alcohol oxidase activity (*SI Appendix*, Fig. S22*B*), including toward sinapyl alcohol to produce sinapaldehyde (Fig. 3*A*). Moreover, addition of proline to the reaction drove nesocodin formation (Fig. 3*B–D*). Sinapyl alcohol, the precursor to sinapaldehyde, was also detected in nectar at very low levels in +24 h nectar (*SI Appendix*, Fig. S23), suggesting it is exported from nectary cells prior to oxidation.

NmNec2 Is a Ferritin-like Catalase. NmNec2 has high similarity to plant "desiccation-related proteins" (*SI Appendix*, Fig. S24). Although of unknown function, plant desiccation-related proteins contain a ferritin-like domain like those found in a

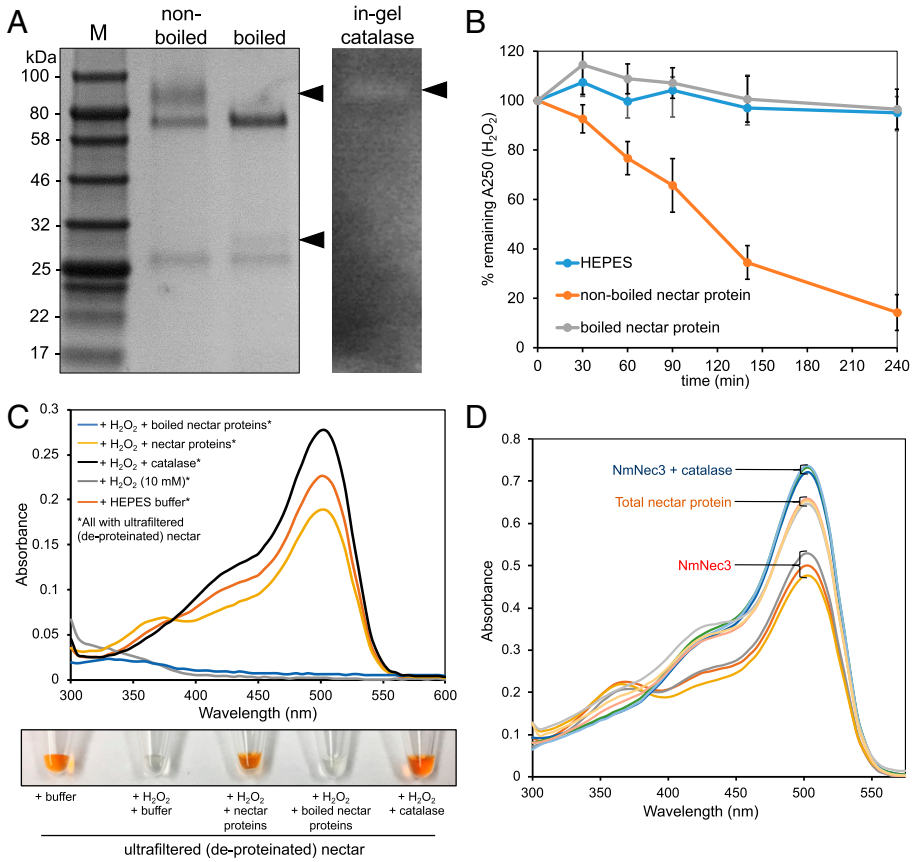

Fig. 4. NmNec2 has catalase activity that can protect nesocodin from H_2O_2-mediated degradation. (*A*) *Left*, SDS-PAGE (4 to 20%) analysis of 18 μL of raw nonboiled and boiled nectar stained with Coomassie blue; *Right*, in-gel catalase assay after SDS-PAGE without sample boiling or addition of reducing agent. Arrowheads indicate location of NmNec3 and associated activity band. (*B*) Catalase activity of total nonboiled (orange line) or boiled (gray) nectar proteins. Assays contained 25 mM H_2O_2 in 50 mM HEPES (pH 8.0) and either 0.17 μg/μL of total nectar proteins (either boiled or nonboiled) or an equivalent volume of HEPES buffer as a negative control. (*C*) Catalase-mediated protection of natural nesocodin. Filtered (deproteinated) nectar was incubated with 10 mM H_2O_2 for 18 h with either total nonboiled (yellow line) or boiled (blue) nectar proteins (0.1 μg/mL final). Controls included the addition of heme-based catalase (green), no protein (gray), and no H_2O_2 added [orange, "+HEPES" (25 mM, pH 8.0)]. (*D*) Catalase-mediated protection of quasisynthetic nesocodin. All reactions contained 1 mM sinapyl alcohol, 10 mM proline, and 0.1 μg/μL NmNec3 in 50 mM $Na(H)CO_3$ (pH 9.0). A subset of reactions contained either 0.2 μg/μL total nectar protein or 0.1 μg/μL of heme-based catalase. Traces of absorbance spectra from three individual replicates are presented as labeled.

subgroup of bacterial Mn-dependent catalases (21). Catalase dismutates hydrogen peroxide (H_2O_2) into water and O_2(g). We first determined that freshly collected *Nesocodon* nectar has no detectable H_2O_2, suggesting the possibility of active removal, especially since one of the products from NmNec3's alcohol oxidase activity is H_2O_2 (Fig. 3*D*). Subsequent in-gel (Fig. 4*A*) and proteomic analysis (*SI Appendix*, Fig. S25*A*) demonstrated that nonboiled NmNec2 is a multimeric catalase (~90 kDa), which dissociates into monomers upon boiling (~30 kDa) (Fig. 4*A*), consistent with the detergent-resistant, multimeric ferritin-like Mn catalases found in some bacteria (21). Similarly, purified total nectar proteins have catalase activity that is inhibited by boiling (Fig. 4*B*; *SI Appendix*, Fig. S25*B*).

To determine a role for catalase activity in nectar, exogenous H_2O_2 was applied to either ultrafiltered (deproteinated) +24 h nectar or synthetic nesocodin, which degraded the pigment in both cases (Fig. 4*C*; *SI Appendix*, Fig. S25*C*). Conversely, addition of purified nectar proteins (nonboiled) or commercial heme-based catalase protected the pigment (Fig. 4*C*). While the sinapyl alcohol oxidase activity of NmNec3 may be essential for red pigment formation, the H_2O_2 produced by this reaction may limit final nectar color intensity. Indeed, the addition of purified nectar proteins or heme-based catalase to reactions containing NmNec3, sinapyl alcohol, and proline increased the total pigment yield (Fig. 4*D*).

We propose a mechanistic model for nectar pigment synthesis and stability in *Nesocodon* as diagrammed in *SI Appendix*, Fig. S26. Nectar from newly opened flowers is weakly acidic and pale yellow, but its pH progressively increases through the action of a carbonic anhydrase (NmNec1), likely supplied with bicarbonate through nectary respiration. Simultaneously, sinapyl alcohol is exported from nectaries and oxidized to sinapaldehyde by the alcohol oxidase NmNec3. Nectar alkalinization supports 1) condensation of sinapaldehyde with proline to form nesocodin and 2) the deprotonation of both sinapaldehyde and nesocodin, which is required for color formation and stability. Lastly, NmNec2 has catalase activity that protects nesocodin from degradation by the H_2O_2 generated by NmNec3.

Nesocodin Is Visible and Attractive to Day Geckos

The true pollinator of *Nesocodon* flowers is unknown, but several Mauritian species produce colored nectars and are visited and pollinated by day geckos, with even artificially colored synthetic nectars being attractive to *Phelsuma* geckos (13). However, these suggestive observations lack conclusive data linking the specific nectar pigments to the sensory system and behavior of their putative pollinators. To investigate the function of nesocodin as an attractant to day geckos, we used a physiological model of gecko

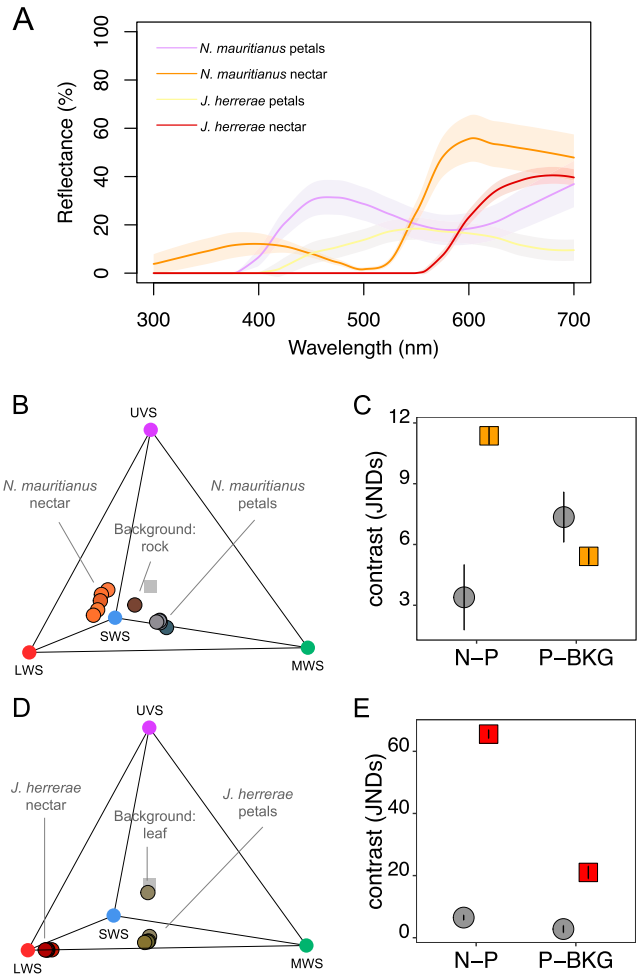

Fig. 5. Nectars containing nesocodin are visible and conspicuous to pollinators (diurnal geckos and birds). (*A*) Reflectance of *N. mauritianus* and *J. herrerae* nectars and the surrounding petals. Shaded areas around the curves represent 1 SD. (*B*) Tetraplot showing *N. mauritianus* reflectance data from *A* projected onto the visual space of diurnal *Phelsuma* geckos. The vertices of the tetrahedron correspond to four different photoreceptors. (*C*) Achromatic contrast (gray points) and chromatic contrast (orange points) between nectar and the adjacent petals (N-P) and petals and the natural rocky background (P-BKG) for *N. mauritianus*. (*D*) Tetraplot showing *J. herrerae* reflectance data from *A* projected onto the visual space of its respective pollinator, the green-backed fire crown hummingbird *S. sephaniodes*. (*E*) Achromatic contrast (gray points) and chromatic contrast (red points) between N-F and P-BKG for *J. herrerae*. Contrasts are expressed in units of JND (just noticeable differences), and the higher the value, the more conspicuous the color should appear to the pollinators. Error bars are 1 SE.

vision and a behavioral experiment to assess the visibility and attractiveness of nesocodin to gold dust day geckos, *Phelsuma laticauda*. We measured nectar reflectance within the context of the surrounding petals (i.e., "flowers" in Fig. 5*A*; note that the reflectance of distantly related *Jaltomata herrerae* flowers with red nectar was also analyzed and further described below) in order to model visibility and conspicuousness with respect to known retinal response patterns (Fig. 5 *B* and *C*). *Phelsuma* geckos have four types of photoreceptors (UV, blue, green, and red), and hence, their visual space can be represented in the form of a tetrahedron, with each vertex corresponding to a specific photoreceptor (22, 23). The reflectance spectrum of *Nesocodon* nectar (Fig. 5*A*) mapped onto this visual space indicated that the red color of the nectar should be visible to *Phelsuma* (Fig. 5*B*). Moreover, the contrast between the nectar and the surrounding petals is highly conspicuous (Fig. 5*C*).

In a behavioral preference test (*SI Appendix*, Fig. S27), *Phelsuma* were allowed to visit and consume two artificial nectars that differed solely in the absence or presence of synthetic nesocodin (*SI Appendix*, Fig. S28) and hence color (noncolored versus red) but were otherwise chemically identical. The geckos not only investigated sources of red nectar containing nesocodin more often than sources of clear nectar without nesocodin, but they also consumed significantly more of the red-colored nectar (Fig. 6 *A* and *B*; *SI Appendix*, Table S1). These cumulative results strongly suggest that nesocodin's red color is both visible and attractive to *Phelsuma* day geckos, thus supporting a role in pollinator attraction as a conspicuous "honest reward," as previously suggested (10, 11, 24, 25).

Convergent Evolution of an Identical Trait in a Hummingbird-Visited Plant

Given the finding of nesocodin in a Mauritian nectar, we investigated the possibility of distantly related species with red-colored nectars also containing similar metabolites. Toward this end, we evaluated the red nectar of *J. herrerae* and the noncolored nectar of one of its close relatives, *Jaltomata procumbens*. *Jaltomata* spp. with red nectars are visited by hummingbirds in the wild, whereas ones with noncolored nectars tend to be visited by insects (26). Furthermore, *J. herrerae* is endemic to the high elevations (~3,000 to 4,000 m) of the mountains of southern Peru and Bolivia (27), and *J. procumbens* is native to a range from Arizona (USA) down to northern South America (28). Estimates of divergence times indicate that *Nesocodon* (Campanulids/Asterids II) and *Jaltomata* (Lamiids/Asterids I) last shared a common ancestor ~104 million years ago (29).

Like *Nesocodon*, *J. herrerae* nectar is highly alkaline (pH ~9) and contains nesocodin (Fig. 7*A*; *SI Appendix*, Fig. S29), whereas *J. procumbens* nectar is acidic (pH ~6) and colorless (Fig. 7*A*). Similarly, *J. herrerae* nectar contains both an α-carbonic anhydrase [α-CA (JhNec5) in Fig. 7 *B* and *C* and *SI Appendix*, Fig. S30] and a sinapyl alcohol oxidase [SAO (JhNec7) in Fig. 7 and *SI Appendix*, Figs. S21 and S31] analogous to the ones found in *Nesocodon* (see below). The acidic nectar of *J. procumbens* also contains an alcohol oxidase but lacks the carbonic anhydrase and associated activity found in both *J. herrerae* (Fig. 7 *B* and *C*) and *Nesocodon* nectars (Fig. 2). Finally, modeling of *J. herrereae* nectar and petal reflectance (Fig. 5*A*) onto the visual space of hummingbirds suggests that the nectar should also be highly visible and conspicuous (Fig. 5 *D* and *E*), as predicted for the *Nesocodon–Phelsuma* system (Fig. 5 *B* and *C*).

While interesting, the finding of nesocodin in both *Nesocodon* and *Jaltomata* nectars could be a conserved or independently evolved trait. Two key pieces of information strongly suggest that a case of convergent evolution has occurred in the production of this nectar pigment in these two members of the long-diverged Campanulaceae (*Nesocodon*) and Solanaceae (*Jaltomata*). Firstly, the carbonic anhydrases found in *Nesocodon* and *J. hererrae* nectars only share ~42% identity (*SI Appendix*, Fig. S30) and have closer homologs in each other's genomes. Secondly, the alcohol oxidases found in *Nesocodon* and *Jaltomata* nectars are clearly not orthologous (~21% identity, *SI Appendix*, Fig. S31), as they belong to two different enzyme families (*SI Appendix*, Fig. S21). Specifically, *Nesocodon* Nec3 (alcohol oxidase) belongs to the GMC flavoenzyme oxidoreductase family, whereas the *Jaltomata* alcohol oxidase is a member of the berberine-bridge family of enzymes within the flavin adenine dinucleotide/flavin mononucleotide (FAD/FMN)-containing dehydrogenase superfamily. These findings strongly suggest that the genes encoding these enzymes have independently evolved to have the same function in pigment formation.

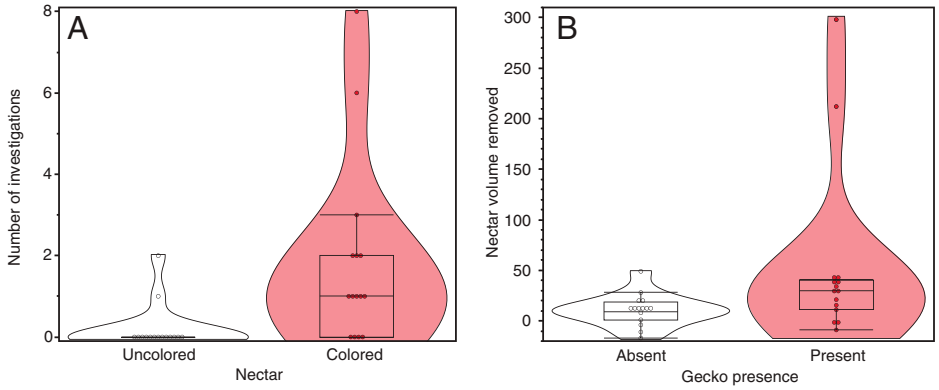

Fig. 6. Nectars containing nesocodin are attractive to diurnal geckos (*Phelsuma*). (*A*) Number of investigations made by geckos ($n = 15$) to tubes containing synthetic nectars with or without 3 mM nesocodin. Sources of nectar with nesocodin were visited significantly more often than sources without nesocodin (Wilcoxon signed-ranks test: W = 60, z = 2.65, two-tailed $P = 0.008$). (*B*) The net volume of nectar removed by geckos ($n = 15$) relative to evaporative control nectars in adjacent terraria without geckos. Significantly more of the nectar with nesocodin was consumed by the geckos (Wilcoxon signed-ranks test: W = 77, z = 2.4, two-tailed $P = 0.0164$). The experimental setup used for this study is graphically illustrated in *SI Appendix*, Fig. S27.

Conclusion

This work cumulatively reports the identification of a convergently evolved plant pigment and its associated synthesis. These findings add to a growing list of convergent evolution in complex biosynthetic pathways (30–33). More specifically, it illustrates how modulation of the nectar chemical environment, largely through action of a carbonic anhydrase, impacts the production of red-colored nectars and how distantly related plants have independently converged on the same biochemical solution of how to produce a red nectar. This red pigment likely functions, at least in part, to attract and direct the vertebrate pollinators these plants rely on in habitats with few potential insect pollinators, like island cliff sides (*Nesocodon* of Mauritius) and mountains (*Jaltomata* in the Andes of South America). Indeed, it has been speculated that geographically isolated areas with numerous vertebrates, but relatively few insects, may have given rise to plant species with colored nectars (25). We anticipate our findings will serve as a starting point for more in-depth comparative biochemical and behavioral studies on pigment-driven plant–pollinator interactions within an evolutionary context.

Materials and Methods

Plant Materials. *N. mauritianus*, *J. herrerae*, and *J. procumbens* were curated and maintained by the College of Biological Sciences Conservatory at the University of Minnesota, St. Paul, Minnesota, USA. Plants were grown with the temperature maintained between 18 and 24 °C.

pH Measurements. Nectar pH was determined by mixing raw nectar 1:1 with 100 μg/mL bromothymol blue dissolved in diH_2O and measuring the absorbance at 613 nm relative to a standard curve consisting of 50 mM buffers at pH 6.5 [2-(N-morpholino)ethanesulfonic acid (MES)], 7.0 [4-(2-hydroxyethyl)-1-piperazineethanesulfonic acid (HEPES), 7.5 (HEPES)], 8.0 (HEPES), 8.5 (Tricine), and 9.0 [tris(hydroxymethyl)methylamino]propanesulfonic acid (TAPS)]. The relative accuracy of pH calculations was either confirmed with colorpHast 5 to

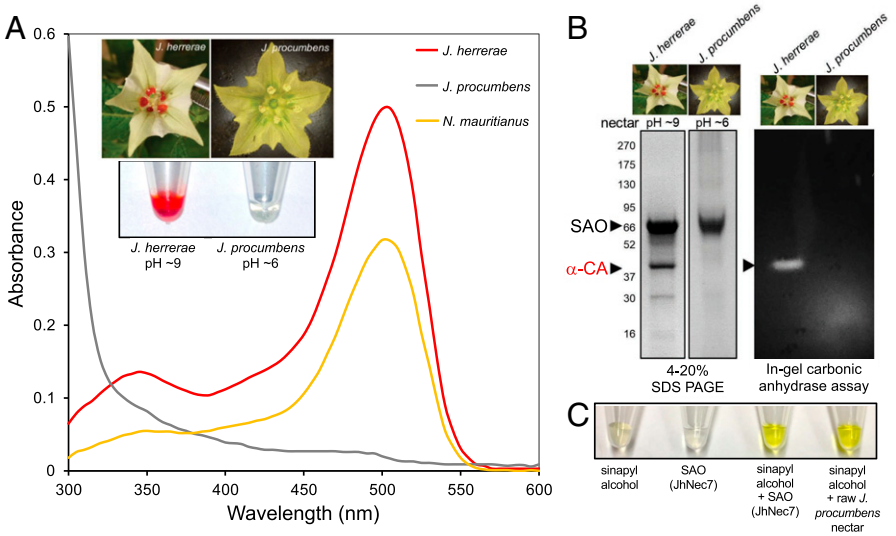

Fig. 7. *J. herrerae* nectar contains nesocodin and analogous enzymes for its production. (*A*) Absorbance spectra of *J. herrerae*, *J. procumbens*, and *N. mauritianus* nectars. *Inset*: *J. herrerae* and *J. procumbens* flowers and nectars. (Note: the spectra of *J. herrereae* and *N. mauritianus* are from samples diluted 1:50, whereas that of *J. procumbens* is not diluted.) (*B*) SDS-PAGE analysis of nectar proteins (*Left* panels) from *J. herrerae* and *J. procumbens* and in-gel carbonic anhydrase activity assays (*Right*). The arrowheads indicate the locations of an α-carbonic anhydrase (α-CA) and sinapyl alcohol oxidase (SAO). (*C*) Sinapyl alcohol oxidase activity in *Jaltomata* nectars. Images of sinapyl alcohol and purified sinapyl alcohol oxidase (SAO; JhNec7) from *J. herrerae* are shown in the left two tubes. The right two tubes show the production of yellow sinapaldehyde after mixing sinapyl alcohol with either purified enzyme from *J. herrerae* or raw nectar from *J. procumbens* (note: *J. procumbens* produces too little nectar to allow for purification of the enzyme prior to the assay).

10 pH strips (EM-Reagents Cat. 9588) or by direct measurement with a Spectrum Technologies Scout 400 pH meter with a blunt tip ion-sensitive field-effect transistor (ISFET) probe by placing the nectar in the rubber storage cap.

UV/Visible Absorbance Spectroscopy. A BioTek PowerWave HT 96-well plate reader or an Implen NanoPhotometer Pearl were used for all spectrophotometric analyses.

Nectar Proteomics. Eighteen microliters of *N. mauritianus* nectar was electrophoresed on a 4 to 20% Tricine gel under denaturing conditions and stained with PAGE-Blue (Thermo Fisher Scientific catalog no. 24620). Protein bands were excised and submitted for identification at the University of Minnesota's Center for Mass Spectrometry and Proteomics Facility. In-gel trypsin digestion and STop And Go Extraction (STAGE) Tip peptide cleanup was performed as previously described (34) except that iodoacetamide was used as the alkylating reagent during the digest protocol. The peptides were analyzed by capillary LC-MS/MS on an Orbitrap Velos system with data dependent acquisition (Orbi-Orbi mode with higher energy collisional dissociation [HCD] activation) as described previously (35). The PEAKS Studio 8.5 (36) (Bioinformatics Solutions) was used for database searching. We formatted a custom protein sequence database from the theoretically translated *Nesocodon* nectary RNA sequencing (RNA-seq) data (NCBI SRA GSE149898) merged with NCBI Reference Sequence *Arabidopsis thaliana* (tax id 3702) downloaded on 5/14/2018 and common laboratory contaminant proteins (from https://www.thegpm.org/crap/). Search parameters were de novo precursor tolerance 20 ppm and fragment ion tolerance 0.1 Da; database search precursor mass tolerance 50.0 ppm; fragment mass error tolerance 0.1 Da; precursor mass search type monoisotopic; trypsin enzyme specificity; fixed modification cysteine carbamidomethylation; variable modifications methionine oxidation, pyroglutamic acid, deamidation of asparagine and glutamine, and protein N-terminal acetylation; maximum variable modifications per peptide 3; false discovery rate calculation on; spectra merge off; charge state correction; and spectral filter quality >0.65. We employed the PEAKS Studio module SPIDER for consideration of amino acid substitutions in the target protein sequence database. The exact same methods were used to identify nectar proteins in the nectar of *J. herrerae* with theoretical translations being derived from RNA-seq data (NCBI SRA accession no. GSE191201).

NmNec3 Purification. For a standard preparation, 250 μL nectar was diluted 1:1 with 50 mM HEPES (pH 8.0), heated for 2 min at 50 °C and then centrifuged through a 50,000 molecular weight cut-off (MWCO) Amicon Ultra-0.5 Centrifugal Filter (Millipore Sigma) for 5 min at 14,000 × *g*, with the remaining ~50 μL of retentate diluted back up to 500 μL in 50 mM HEPES (pH 8.0) and centrifugation repeated four more times. The purity of the final product was evaluated by 10% SDS-PAGE under denaturing conditions and gel staining with PAGE-Blue (Thermo Fisher Scientific catalog no. 24620). Final protein concentration was determined by UV absorbance at 280 nm and a predicted extinction coefficient of 56,520 M^{-1} cm^{-1} (based on the sequence of the mature protein without the predicted signal peptide).

Preparation of Deproteinated (Ultrafiltered) Nectar and Total Nectar Protein. Total protein was removed from 400 μL of raw nectar via centrifugation through a 3,000 MWCO Amicon Ultra-0.5 Centrifugal Filter (Millipore Sigma) for 10 min at 14,000 × *g*. The flow-through was collected as "deproteinated" nectar and validated for protein removal by 4 to 20% SDS-PAGE. Meanwhile, the retentate was brought back up to 400 μL with 50 mM HEPES (pH 8.0) and recentrifuged and washed a total of five times to remove nectar sugars and other small molecule components.

Enzymatic Assays.

In-gel carbonic anhydrase assay. Fresh *Nesocodon* nectar was collected, and 18 μL was immediately subjected to standard SDS-PAGE (4 to 20%), except the loading buffer contained no β-mercaptoethanol and the samples were not boiled prior to loading the gel. Following electrophoresis, the gel was sliced vertically with one lane being stained in PageBlue and the remaining lanes being processed for an in-gel carbonic anhydrase activity assay as previously described (37), except that dry ice was used to bubble CO_2 into the distilled water instead of a compressed CO_2 tank. The positive control carbonic anhydrase was purchased from Millipore Sigma (C9207-1VL).

Colorimetric carbonic anhydrase assay. Assays with raw 0 h nectar contained either carbonic anhydrase inhibitors (acetazolamide, sulfanilamide, or 6-ethoxy-2-benzothiazolesulfonamide) or an equivalent amount of dimethyl sulfoxide (DMSO) (10% DMSO [vol/vol] for acetazolamide and sulfanilamide, 50% DMSO [vol/vol] for 6-ethoxy-2-benzothiazolesulfonamide). Reactions were initiated by adding $NaHCO_3$ (pH 7.45) at a final concentration of 4 mM, with the absorbance at 420 nm (positively correlating to an increase in pH) being monitored for 3 min. Assays recapitulating that of raw nectar contained 125 μM sinapaldehyde in 5 mM $NaHCO_3$ (5 mM final) either with or without commercial carbonic anhydrase (Millipore Sigma C9207-1VL) added.

Sinapyl alcohol oxidase assay. Reactions consisted of 1 mM sinapyl alcohol and 0.1 mg/mL NmNec3 in 50 mM Na(H)CO_3 (pH 9.0) incubated at 21 °C for 30 min followed by conducting wavelength scans of 300 to 600 nm. Negative controls with sinapyl alcohol but no NmNec3 did not yield any sinapaldehyde (gray line); a 0.5 mM sinapaldehyde standard in 50 mM Na(H)CO_3 (pH 9.0) was used as a reference.

In-gel alcohol oxidase assay. First, 12 μL of raw nectar was directly loaded (no loading buffer) into separate lanes of a 4 to 20% Tricine PAGE gel and electrophoresed under nondenaturing conditions at 120 V for ~1 h. The gel was then incubated at 37 °C in a staining solution containing 25 mM Tris (pH 8.2) and 10% methanol (MeOH), 10% ethanol (EtOH), 10% 1-propanol, 10% 2-propanol, or 5 mM sinapyl alcohol, along with 5 U/mL horseradish peroxidase, 0.5 mg/mL 3,3′ diaminobenzidine, and 0.1 mg/mL flavin adenine dinucleotide for ~3 h.

In-gel catalase assay. First, 18 μL of fresh, raw nectar was electrophoresed on a 4 to 20% Tricine gel in the presence of SDS, but without boiling or β-mercaptoethanol. Catalase activity was detected in the gel as previously described (38).

Spectrophotometric catalase assay. Assays were performed by monitoring the breakdown of H_2O_2 by measuring the absorbance at 250 nm (39). Briefly, individual assays contained 25 mM H_2O_2 in 50 mM HEPES (pH 8.0) and either 0.17 mg/mL of total nectar proteins (either boiled or nonnboiled) or an equivalent volume of HEPES buffer as a negative control, and the absorbance was monitored at 250 nm over time.

In situ pharmacological treatments. Individual nectar droplets from newly opened flowers (0 h) were treated by the addition of carbonic anhydrase inhibitors (acetazolamide, sulfanilamide, or 6-ethoxy-2-benzothiazolesulfonamide) or equivalent amounts of DMSO (10% DMSO [vol/vol] for acetazolamide and sulfanilamide, 50% DMSO [vol/vol] for 6-ethoxy-2-benzothiazolesulfonamide) and thorough mixing by repeated pipetting. After 8 to 20 h, nectar was removed and analyzed for pH and subjected to absorbance wavelength scans.

Fluorescence Spectroscopy. Raw nectar and synthetic nesocodin (sinapaldehyde + proline) were diluted 1:99 in 25 mM HEPES (pH 8.0), and the excitation and emission spectra were measured with a BioTek Synergy MX Microplate Reader.

Thin-Layer Chromatography of Synthetic Nesocodin. For chromatography, 2 μL each of synthetic nesocodin (1 mM sinapaldehyde + 10 mM proline in 50 mM HEPES [pH 8.0]), raw nectar, or 1 mM sinapaldehyde alone were spotted onto silica gel-on-glass thin-layer chromatography (TLC) plates (Millipore Sigma Z12,268-8) with a mobile phase of 100 mM sodium acetate (pH 4.8) being used under ambient air. Plates were air dried and imaged under UV light (340 nm).

LC-High-Resolution Mass Spectrometry Analysis. Chromatographic separation and high-resolution mass spectral analyses of *Nesocodon* nectar and synthetic nesocodin were performed using a UHPLC coupled to a hybrid quadrupole-Orbitrap mass spectrometer (Ultimate 3000 HPLC, Q Exactive, Thermo Fisher Scientific). The UHPLC is equipped with a flow-through photo diode array detector allowing concurrent UV/visible spectrophotometric and MS analysis of separated analytes postcolumn. Nectar samples were first purified by C_{18} solid phase extraction using a Ziptip (Millipore Sigma) conditioned in ~20 μL of acetonitrile, washed with 20 μL of 0.1% formic acid in water, loaded with ~20 μL of nectar, and washed with ~100 μL of 0.1% formic acid in water prior to elution with ~10 μL of acetonitrile. The eluate was then transferred into LC-MS autosampler vials, and 1 μL was injected (via autosampler) onto a reversed-phase C_{18} HSS T3 1.8 μm particle size, 2.1 × 100 mm column (Waters). The column temperature was 40 °C and the solvent flow rate 0.45 mL/min. A 20-min linear gradient using mobile phases A, 0.1% formic acid in water, and B, 0.1% formic acid in acetonitrile, was run according to the following gradient 25-min elution profile: initial, 2% B; 20 min, 98% B; 21 min, 98% B; 22 min, 2% B (hold to 25 min). The following MS conditions were used: full scan mass scan range, 100 to 1,000 *m/z*; resolution, 70,000; data type profile, desolvation temperature 350 °C; capillary voltage, 3,800 V (+), 4,000 V (−). Xcalibur software version 2.1 (Thermo Fisher Scientific) was used to record and visualize the chromatograms and spectra. Tandem MS (MS/MS) spectra of nectar-derived sinapaldehyde and nesocodin were sequentially fragmented in the HCD collision cell with normalized collision energies of 10, 20, 25, 30, 35, and 40%. MS/MS scans were acquired with 17,500 resolution, and the target value was 2.0×10^5 with 100 ms of maximum injection time. An isolation width of 2.0 *m/z* was used for precursor ion selection in MS/MS mode.

Proline Quantification. Proline in *Nesocodon* nectar was quantified using isotope dilution and a gas chromatography (GC)-MS–based amino acid analysis method (40). Briefly, three 100-μL aliquots of red (+48 h) *Nesocodon* nectar were prepared and 99 atom% ^{13}C L-[$^{13}C_5$]proline (604801; Millipore Sigma) was added to a concentration of 10 mM. The samples were acidified by adding 1 mL of 0.01 M HCl and amino acids were loaded by addition to a strong cation exchange solid phase extraction (SPE) column (AT209800, Alltech) preconditioned with 1 mL of 0.01 M HCl and three additions of 1 mL of diH_2O. Once loaded, the SPE columns were washed twice with 1 mL of 80% (vol/vol) methanol in water before amino acids were eluted with 250 μL of a 1:1 (vol/vol) mixture of 8 M NH_4OH and methanol. Aliquots (50 μL) of each eluate in dry glass vials were derivatized by adding 5 μL of pyridine (Millipore Sigma) and 5 μL of methyl chloroformate (Millipore Sigma). The reactions were allowed to proceed for 1 min before 90 μL of chloroform and 90 μL of 50 mM sodium bicarbonate in water were added to stop the reaction. The chloroform layers were removed and dried over anhydrous sodium sulfate prior to GC-MS analysis. GC-MS was performed on a 7890A/5973 MSD instrument (Agilent) using 1 μL sample injection volume in splitless mode, a DB-5 ms ultrainert (30 m, 0.25 mm inner diameter, 0.25 μm film thickness) capillary GC column, inlet temperature of 240 °C, and interface temperature of 290 °C. The initial oven temperature was 70 °C and was held for 3 min following injection and was increased at a rate of 25 °C/min to 280 °C where it was held for 5 min before returning to initial settings. Data were analyzed using ChemStation software.

In parallel experiments, proline in 0 h and +24 h nectar was evaluated by thin-layer chromatography. In brief, 2 μL total (in 1-μL increments) of 0 h and +24 h were spotted onto 10 × 10 cm High-performance TLC (HPTLC) cellulose-on-glass plates (Merck 1.05787.0001). After airing drying the spotted plates, separation was performed in an airtight glass container with a mobile phase of 60:25:15 of 1-butanol:H_2O:acetic acid. Plates were then air dried and developed by spraying with 0.3% ninhydrin in 1-butanol/3% acetic acid. Proline reaction with ninhydrin uniquely develops as a yellow product, whereas most other amino acids generate a purple or red products.

Nesocodin Derivatization by Reduction with $NaBH_4$ or $NaBD_4$. Nesocodin was synthesized in a 1-mL reaction containing 10 mM proline and 1 mM sinapaldehyde in 50 mM Na(H)CO_3 buffer (pH 9.0). The reaction started to turn visibly red immediately and was allowed to incubate at 21 °C for 30 min prior to being divided into three equal aliquots (330 μL each). Additions of 23 mg of $NaBH_4$ and 22 mg of $NaBD_4$ were made to the first and second aliquots, respectively. The reductant was in excess of sinapaldehyde concentration by over three orders of magnitude, with ∼1.8 M $NaBH_4$ and ∼1.6 M $NaBD_4$. Both reduced aliquots bubbled immediately upon addition of the solid reducing agent but stopped after a few seconds. Reaction tubes were capped and mixed by inversion and then uncapped to release residual pressure. Within the mixing time, both reduced aliquots became colorless. The third, red aliquot was reserved as a negative control. All three aliquots were acidified by addition of 330 μL of 1% (vol/vol) formic acid in water. The first two aliquots bubbled upon addition of the acid and were allowed to react for several minutes uncapped before proceeding. All three aliquots were first purified by C_{18} solid phase extraction using an OMIX 100-μL tip (Agilent) conditioned in ∼200 μL of 90% (vol/vol) methanol in water with 0.1% (vol/vol) formic acid, washed with 200 μL of 0.085% formic acid in water, loaded with ∼600 μL of each aliquot, and washed three times with 100 μL of 0.085% formic acid in water prior to elution with ∼20 μL of 90% (vol/vol) methanol in water with 0.1% (vol/vol) formic acid. Samples were subsequently analyzed by LC-HRMS as described above.

Nesocodin Synthesis for Structural Validation. For NMR and other structural analyses, nesocodin was prepared by dissolving 223.9 mg (1.086 mmol) of sinapaldehyde in 10 mL methanol (to 0.1086 M) and then adding 125.0 mg of L-proline (1.086 mmol) followed by a substoichiometric addition (100 μL, ∼0.42 mmol) of tributylamine (as a sterically hindered base catalyst with low nucleophilicity). As the mixture is allowed to react, a yellow-to-red color change is observable immediately, and the reaction runs to completion within minutes at room temperature. Once the reaction is complete, the contents of the reaction flask are diluted 10-fold into room-temperature ethyl acetate. A red solid precipitate consisting of a 64% E- to 36% Z-mixture of nesocodin isomers was collected by filtration, washed with a small volume of ice-cold ethyl acetate, and dried in vacuo overnight.

Synthetic Nesocodin NMR. First, 1 mg of the dried red solid nesocodin was dissolved in one mL of methanol-d_4 containing 0.1% tetramethylsilane as an internal standard and transferred into a 5-mm thin-walled quartz NMR tube (Wilmad 535-PP-7). NMR data including one-dimensional (1D) ^1H-NMR (*SI Appendix*, Fig. S11), two-dimensional ^1H-double-quantum filtered correlation spectroscopy-NMR (2D ^1H-DQF-COSY) (*SI Appendix*, Fig. S12), 1D ^{13}C-NMR (with and without ^1H decoupling) (*SI Appendix*, Fig. S13), two-dimensional heteronuclear single quantum coherence-NMR (2D HSQC-NMR) (*SI Appendix*, Fig. S13*B*), and two-dimensional Nuclear Overhauser Effect Spectroscopy-NMR (2D NOESY-NMR) (*SI Appendix*, Fig. S14) were obtained on a Bruker 600 MHz NMR at the University of Minnesota NMR Center on a fee-for-service basis and analyzed using TopSpin version 4.0.6.

RT-PCR Analysis. Total RNA from frozen samples was extracted using TRIzol RNA Reagent (Sigma-Aldrich). The RNA was treated with TURBO DNA-free kit (Invitrogen) according to the manufacturer's protocol. First-strand complementary DNA (cDNA) was synthesized from 1 μg of total RNA using iScript cDNA synthesis kit (Bio-Rad). RT-PCR was performed with GoTaq DNA polymerase (Promega). The *NmGAPDH* gene was used as an internal control. For PCR, the primers used for RT-PCR are listed in *SI Appendix*, Fig. S17.

Nectary Transcriptomics Analyses. *Nesocodon* and *Jaltomata* nectary tissues were manually dissected, and total RNA was extracted using TRIzol RNA Reagent (Sigma-Aldrich). The RNA was treated with the TURBO DNA-free kit (Invitrogen) according to the manufacturer's protocol and submitted to the University of Minnesota Genomics Center for messenger RNA (mRNA) isolation, barcoded library creation, and either Illumina HiSeq 2500 sequencing via paired-end 125-bp runs (for *Nesocodon*) or NovaSeq 6000 using via paired-end 150-bp runs (*Jaltomata*) using rapid chemistry. Trinity version 2.4.0 (41) was used to assemble contigs from the reads de novo.

Nectar Protein Maximum Likelihood Tree Generation. Protein sequences were aligned with MUSCLE 3.8.31 (42) and refined with GBLOCKS 0.91b (43). Phylogenetic trees were computed with PhyML 3.1 using the Whelan and Goldman matrix with four gamma-distributed rate categories (44) and edited using the Environment for Tree Exploration toolkit (45).

Behavioral Testing. All capture, handling, and experimental protocols were approved by Institutional Animal Care and Use Committee at George Mason University (IACUC protocol no. 1478025) and were carried out in accordance with all relevant guidelines and regulations.

Fifteen individuals (eight adult females, six adult males, one juvenile) of the Malagasy gold dust day gecko (*P. laticauda*) were used as subjects in a behavioral experiment based on a two-alternative choice test to investigate nectar color preference (*SI Appendix*, Table S1). As in other species belonging to the same genus, gold dust day geckos eat pollen and nectar from flowers in their natural environment in Madagascar (46). All tested animals were collected from wild populations, and they were housed in the same room at George Mason University in the laboratory of one of the authors (Y.C.). All geckos were housed separately in glass terraria (Exoterra, 30 × 30 × 45 cm, W × D × H), exposed to 12:12 h light:dark cycles, and given access to additional light from UV lamps (ReptiSun 10 UVB bulbs). Opaque barriers were placed between terraria to prevent the geckos from seeing individuals in adjacent terraria. The room temperature was maintained between 24.5 and 26.5 °C. Each terrarium contained one or more fake plants and a heat pad for thermoregulation. The humidity level and temperature in the room, as well as the health of each gecko, were monitored daily. Over the course of this study, no gecko showed signs of stress or health problems (e.g., pale coloration or emaciation), and all geckos continued to exhibit normal, species-typical behaviors in their home terraria. No geckos were tested while they were shedding. Water was accessible at all times in a shallow bowl in each terrarium. Geckos were fed three times each week with a combination of crickets dusted with calcium and vitamins, mealworms, and a fruit supplement. Feeding for an experimental subject was temporarily suspended for 3 or 4 d prior to the day it was tested, and the normal feeding regime was resumed immediately after testing of that subject was completed.

Experiments were carried out in a dedicated testing room during the 12-h light portion of the light:dark cycle and always started at the same approximate time (11:00 h). Temperature in the experimental room was recorded at the beginning and end of each experiment and was stable at ∼25 °C over the entire length of the study. Animals were always handled by the same person (author N.M.), and no one else had access to the tested animals and the testing room over the duration of the study. Animals were tested individually and in a single choice test, with only one animal tested on a single day. No food or water—besides the nectars being tested—were provided during a choice test, which lasted 3 h 45 min.

The experimental setup consisted of two identical, custom-made arenas (61.5 × 30.5 × 21 cm, L × W × H) placed next to each other on the floor of the testing room. Each arena was constructed from Plexiglas and consisted of a floor, four walls, a removable lid, a removable transparent barrier (30.5 × 21 cm, L × H) bisecting the arena along its long axis into a habituation zone

and a choice zone, and a fixed transparent barrier (18 × 21 cm, L × H) dividing one end of the arena into two stimulus chambers (*SI Appendix*, Fig. S27). The floor and outside walls of each arena were covered with white paper to avoid distractions during testing. On opposite walls of the two stimulus chambers of each arena, we affixed 1.5-mL Eppendorf tubes that were used for stimulus delivery (*SI Appendix*, Fig. S27). The stimuli consisted of synthetic red-colored versus noncolored nectars. Synthetic nectars, with and without nesocodin (colored and noncolored, respectively), contained 20% sucrose (wt/vol), 10 mM proline, and 1 mM Tricine (pH 8.5), with or without 3 mM nesocodin (pigment), with the final pH being adjusted to 9.0 in order to match the absorbance spectrum of a freshly collected nectar sample (*SI Appendix*, Fig. S28). Nectar was preserved frozen in aliquots until the day before it was used in a choice test, when it was placed in a refrigerator. One of the two arenas was designated as the "test arena" in which behavioral choice tests were conducted. Two video-cameras were placed at the two ends of the test arena to record a gecko's behavior over the entire duration of a choice trial from different camera views (*SI Appendix*, Fig. S27 and Movie S1). The other arena was designated as a "control arena"; its sole purpose was to control for the possibility that colored and noncolored nectars evaporated at different rates during the choice test (i.e., over 3 h 45 min). Over the duration of a choice test, the overhead lights in the room were the only source of light (luminosity in the testing room was measured at 282 lx).

Prior to beginning a choice test, four new Eppendorf tubes were mounted in the test and control arenas, and new aliquots of nectar were removed from the refrigerator and used to fill each Eppendorf tube using a pipettor. Thus, both the test and control arenas contained one Eppendorf tube filled to the top (1.6 mL) with colored nectar and one Eppendorf tube filled to the top (1.6 mL) with noncolored nectar (*SI Appendix*, Fig. S27). The side of the arena on which the colored nectar was placed was randomly determined for each tested gecko and was the same in both arenas. To begin a choice test, the subject was released into the habituation zone of the test arena from a fixed release point (*SI Appendix*, Fig. S27) to begin a 45-min habituation phase during which the gecko was free to explore and acclimate to the new environment of the test arena. The removable transparent barrier bisecting the arena was in place during the habituation phase, allowing the gecko to see the stimuli without being able to access them. At the end of the habituation phase, the removable transparent barrier was removed to commence a 3-h choice phase, during which the gecko was able to move around the entire test arena. No one was in the testing room during the habituation and choice phases except to remove the transparent barrier at the end of the habituation phase. At the conclusion of the choice test, we used a pipettor to measure the volume of nectar that remained in each Eppendorf tube in both the test and control arenas. Following these measurements, the Eppendorf tubes were discarded, and the test arena was washed with soap and hot water to remove any scent or biological marking left by the tested gecko.

Visual Modeling of Day Geckos and Hummingbirds. To examine what role petal and nectar colors play in pollinator attraction, we generated visual models of day gecko and hummingbird vision. Visual models allowed us to answer two crucial questions about pollinator attraction: 1) Can pollinators perceive petal and nectar colors? 2) How conspicuous do these colors appear to pollinator given their specific visual capacities (34)? To construct visual models, we used published cone sensitivities of two day gecko species, *P. inunguis* and *Phelsuma madagascariensis longinsulae* (ultraviolet sensitive [UVS] λ_{max} = 380, short wave sensitive [SWS] λ_{max}= 437, medium wave sensitive [MWS] λ_{max}= 470, longwave sensitive [LWS] λ_{max}= 560; ratio of UVS:SWS:MWS:LWS = 1:1:3.5:6) and the green-backed fire crown hummingbird *Sephanoides sephaniodes* (UVS λ_{max} = 371, SWS λ_{max}= 444, MWS λ_{max}= 504, LWS λ_{max}= 560; ratio of UVS:SWS:MWS:LWS = 1:2:2:4) (22, 23, 47). For both *Phelsuma* species and *S. sephaniodes,* we were unable to find data on cone abundance. Hence, we used cone abundance data from diurnal agamid (*Ctenophorus ornatus*) and chicken (*Gallus gallus domesticus*) as substitutes for *Phelsuma* species and *S. sephaniodes*, respectively (23, 48). For visual modeling, we used receptor-noise limited models, set the irradiance conditions to bright daylight ("D65"), and applied von Kries transformation to account for light adaptation (49, 50). Subsequently, we measured the reflectance of *N. mauritianus* and *J. herrerae* petals and nectar (n = 5 flowers each) using a UV-visible spectrophotometer (OceanOptic JAZ-A2474 with pulsed xenon lamp). Reflectance was measured by setting the triggering rate of the PX lamp to 10 ms and the boxcar to 5. The spectral probe was maintained at an angle of 45° against the petals, which were placed on black velvet paper. This records the reflectance of an ~3 × 3 mm region of the petals. For nectar, 200 μL freshly collected nectar was transferred onto a tissue paper and allowed to dry. Subsequently, reflectance data of the dried nectar was recorded using the same protocol used for measuring reflectance of petals. All measurements were corrected against white and black reflectance standards. These spectral data were then imported in R and smoothened (α = 0.20 or 0.35), and negative values were fixed to "0" using the "fixneg" function in the "pavo2.0" R package (51). These spectra were then projected onto the pollinator-specific visual space generated using photoreceptor sensitivities (see above). Day geckos and hummingbirds both have four distinct photoreceptor types, and hence, their visual spaces can be represented as tetrahedrons whose vertices correspond to each of the four photoreceptors (Fig. 5 *B* and *D*). The location of petal and nectar spectra (represented as individual points) in this visual space depend on the estimated stimulation of each cone type in response to these spectra. Spectra that fall within the tetrahedral space lie within the perceptual range of the pollinator and their corresponding colors can be perceived by pollinators. We found that the spectra of petals and nectar of both *N. mauritianus* and *J. herrerae* lie within visual spaces of day gecko and hummingbird, respectively (Fig. 5*B* and *D*). This indicates that day geckos and hummingbirds can indeed perceive the red nectar and colored petals of *N. mauritianus* and *J. herrerae*.

Data Availability. RNA-seq data for *N. mauritianus* and *J. herrerae* nectary tissues are available at the NCBI SRA (https://www.ncbi.nlm.nih.gov/sra) under the accession numbers GSE149898 and GSE191201, respectively. The mass spectrometry proteomics data have been deposited to the ProteomeXchange Consortium via the PRoteomics IDEntifications Database (PRIDE) partner repository with the dataset identifier PXD029394 and 10.6019/PXD029394 for *N. mauritianus* and PXD029395 and 10.6019/PXD029395 for *J. herrerae*. GenBank accession numbers for the cloned cDNAs are as follows: NmNec1, OK664972; NmNec2, OK664973; NmNec3, OK664974; JhNec5, OL415498; JhNec7, OL504752. Samples of *Nesocodon* and *Jaltomata* nectars are available upon request.

ACKNOWLEDGMENTS. The authors recognize the Center for Mass Spectrometry and Proteomics at the University of Minnesota and various supporting agencies, including the NSF for Major Research Instrumentation grants 9871237 and NSF-DBI-0215759 used to purchase the instruments described in this study. We thank the Minnesota NMR Center (with support from the National Institute of General Medical Sciences [1S10OD021536 (G. Veglia)] for access to NMR instrumentation, as well as the University of Minnesota Genomics Center for conducting RNA quality control, RNA-seq library creation, next-generation sequencing, and primary NGS data QC. We also thank Lisa Aston-Philander, Angie Koebler, and Alex Eilts of the CBS Conservatory and Botanical Collection of the University of Minnesota for helpful discussions and access to plant materials. This work was supported by grants from the US NSF to M.H. and C.J.C. (IOS-1339246); E.C.S.-R., M.H., A.D.H., and C.J.C. (IOS-2025297); and A.D.H. (IOS-1238812). R.R. was supported by a postdoctoral fellowship from the United States Department of Agriculture (2018-67012-28038).

1. M. C. P. P. Reis-Mansur *et al.*, Carotenoids from UV-resistant Antarctic Microbacterium sp. LEMMJ01. *Sci. Rep.* **9**, 9554 (2019).
2. J. Chory *et al.*, From seed germination to flowering, light controls plant development via the pigment phytochrome. *Proc. Natl. Acad. Sci. U.S.A.* **93**, 12066–12071 (1996).
3. I. C. Cuthill *et al.*, The biology of color. *Science* **357**, eaan0221 (2017).
4. H. M. Schaefer, V. Schaefer, D. J. Levey, How plant-animal interactions signal new insights in communication. *Trends Ecol. Evol.* **19**, 577–584 (2004).
5. E. Moyroud, B. J. Glover, The evolution of diverse floral morphologies. *Curr. Biol.* **27**, R941–R951 (2017).
6. M. T. Clegg, M. L. Durbin, Flower color variation: A model for the experimental study of evolution. *Proc. Natl. Acad. Sci. U.S.A.* **97**, 7016–7023 (2000).
7. R. A. Raguso, R. A. Levin, S. E. Foose, M. W. Holmberg, L. A. McDade, Fragrance chemistry, nocturnal rhythms and pollination "syndromes" in *Nicotiana*. *Phytochemistry* **63**, 265–284 (2003).
8. M. Vanderplanck *et al.*, The importance of pollen chemistry in evolutionary host shifts of bees. *Sci. Rep.* **7**, 43058 (2017).
9. A. G. Dyer *et al.*, Parallel evolution of angiosperm colour signals: Common evolutionary pressures linked to hymenopteran vision. *Proc. Biol. Sci.* **279**, 3606–3615 (2012).
10. D. M. Hansen, J. M. Olesen, T. Mione, S. D. Johnson, C. B. Müller, Coloured nectar: Distribution, ecology, and evolution of an enigmatic floral trait. *Biol. Rev. Camb. Philos. Soc.* **82**, 83–111 (2007).
11. F. P. Zhang, Z. Larson-Rabin, D. Z. Li, H. Wang, Colored nectar as an honest signal in plant-animal interactions. *Plant Signal. Behav.* **7**, 811–812 (2012).
12. J. M. Olesen *et al.*, Mauritian red nectar remains a mystery. *Nature* **393**, 529 (1998).
13. D. M. Hansen, K. Beer, C. B. Müller, Mauritian coloured nectar no longer a mystery: A visual signal for lizard pollinators. *Biol. Lett.* **2**, 165–168 (2006).
14. F. P. Zhang *et al.*, Dark purple nectar as a foraging signal in a bird-pollinated Himalayan plant. *New Phytol.* **193**, 188–195 (2012).
15. S. H. Luo *et al.*, Unique proline-benzoquinone pigment from the colored nectar of "bird's Coca cola tree" functions in bird attractions. *Org. Lett.* **14**, 4146–4149 (2012).

16. R. Van Acker *et al.*, Different routes for conifer- and sinapaldehyde and higher saccharification upon deficiency in the dehydrogenase CAD1. *Plant Physiol.* **175**, 1018–1039 (2017).
17. C. Carter, S. Shafir, L. Yehonatan, R. G. Palmer, R. Thornburg, A novel role for proline in plant floral nectars. *Naturwissenschaften* **93**, 72–79 (2006).
18. Y. R. Mo, S. D. Peyerimhoff, Theoretical analysis of electronic delocalization. *J. Chem. Phys.* **109**, 1687–1697 (1998).
19. P. J. Linser, K. E. Smith, T. J. Seron, M. Neira Oviedo, Carbonic anhydrases and anion transport in mosquito midgut pH regulation. *J. Exp. Biol.* **212**, 1662–1671 (2009).
20. L. Sützl, G. Foley, E. M. J. Gillam, M. Bodén, D. Haltrich, The GMC superfamily of oxidoreductases revisited: Analysis and evolution of fungal GMC oxidoreductases. *Biotechnol. Biofuels* **12**, 118 (2019).
21. J. W. Whittaker, Non-heme manganese catalase—The 'other' catalase. *Arch. Biochem. Biophys.* **525**, 111–120 (2012).
22. G. B. Arden, K. Tansley, The electroretinogram of a diurnal gecko. *J. Gen. Physiol.* **45**, 1145–1161 (1962).
23. Y. Taniguchi, O. Hisatomi, M. Yoshida, F. Tokunaga, Pinopsin expressed in the retinal photoreceptors of a diurnal gecko. *FEBS Lett.* **496**, 69–74 (2001).
24. K. Ito, M. F. Suzuki, K. Mochizuki, Evolution of honest reward signal in flowers. *Proc. Biol. Sci.* **288**, 20202848 (2021).
25. I. A. Minnaar, A. Kohler, C. Purchase, S. W. Nicolson, Coloured and toxic nectar: Feeding choices of the Madagascar Giant Day Gecko, *Phelsuma grandis*. *Ethology* **119**, 417–426 (2013).
26. K. C. Plourd, T. Mione, Pollination does not affect floral nectar production, and is required for fruit-set by a hummingbird-visited Andean plant species. *Phytologia* **98**, 313–317 (2016).
27. T. Mione, Jaltomata II: New combinations for five South American species (Solanaceae). *Brittonia* **51**, 31–33 (1999).
28. T. Mione, G. J. Anderson, Genetics of floral traits of *Jaltomata procumbens* (Solanaceae). *Brittonia* **69**, 1–10 (2017).
29. S. Kumar, G. Stecher, M. Suleski, S. B. Hedges, TimeTree: A resource for timelines, timetrees, and divergence times. *Mol. Biol. Evol.* **34**, 1812–1819 (2017).
30. R. Huang, A. J. O'Donnell, J. J. Barboline, T. J. Barkman, Convergent evolution of caffeine in plants by co-option of exapted ancestral enzymes. *Proc. Natl. Acad. Sci. U.S.A.* **113**, 10613–10618 (2016).
31. K. Heyduk, J. J. Moreno-Villena, I. S. Gilman, P. A. Christin, E. J. Edwards, The genetics of convergent evolution: Insights from plant photosynthesis. *Nat. Rev. Genet.* **20**, 485–493 (2019).
32. R. Greenway *et al.*, Convergent evolution of conserved mitochondrial pathways underlies repeated adaptation to extreme environments. *Proc. Natl. Acad. Sci. U.S.A.* **117**, 16424–16430 (2020).
33. N. B. Jensen *et al.*, Convergent evolution in biosynthesis of cyanogenic defence compounds in plants and insects. *Nat. Commun.* **2**, 273 (2011).
34. Y. M. Thu *et al.*, Slx5/Slx8 promotes replication stress tolerance by facilitating mitotic progression. *Cell Rep.* **15**, 1254–1265 (2016).
35. Y. Lin-Moshier *et al.*, Re-evaluation of the role of calcium homeostasis endoplasmic reticulum protein (CHERP) in cellular calcium signaling. *J. Biol. Chem.* **288**, 355–367 (2013).
36. B. Ma *et al.*, PEAKS: Powerful software for peptide de novo sequencing by tandem mass spectrometry. *Rapid Commun. Mass Spectrom.* **17**, 2337–2342 (2003).
37. V. De Luca, S. Del Prete, C. T. Supuran, C. Capasso, Protonography, a new technique for the analysis of carbonic anhydrase activity. *J. Enzyme Inhib. Med. Chem.* **30**, 277–282 (2015).
38. C. J. Weydert, J. J. Cullen, Measurement of superoxide dismutase, catalase and glutathione peroxidase in cultured cells and tissue. *Nat. Protoc.* **5**, 51–66 (2010).
39. R. F. Beers Jr., I. W. Sizer, A spectrophotometric method for measuring the breakdown of hydrogen peroxide by catalase. *J. Biol. Chem.* **195**, 133–140 (1952).
40. W. I. Menzel, W. P. Chen, A. D. Hegeman, J. D. Cohen, Qualitative and quantitative screening of amino acids in plant tissues. *Methods Mol. Biol.* **918**, 165–178 (2012).
41. M. G. Grabherr *et al.*, Full-length transcriptome assembly from RNA-Seq data without a reference genome. *Nat. Biotechnol.* **29**, 644–652 (2011).
42. R. C. Edgar, MUSCLE: Multiple sequence alignment with high accuracy and high throughput. *Nucleic Acids Res.* **32**, 1792–1797 (2004).
43. G. Talavera, J. Castresana, Improvement of phylogenies after removing divergent and ambiguously aligned blocks from protein sequence alignments. *Syst. Biol.* **56**, 564–577 (2007).
44. S. Guindon *et al.*, New algorithms and methods to estimate maximum-likelihood phylogenies: Assessing the performance of PhyML 3.0. *Syst. Biol.* **59**, 307–321 (2010).
45. J. Huerta-Cepas, F. Serra, P. Bork, ETE 3: Reconstruction, analysis, and visualization of phylogenomic data. *Mol. Biol. Evol.* **33**, 1635–1638 (2016).
46. M. Calvino-Cancela, *Phelsuma laticauda laticauda* (Golden dust day gecko) Nectarivory. *Herpetol. Rev.* **36**, 182–183 (2005).
47. G. Herrera *et al.*, Spectral sensitivities of photoreceptors and their role in colour discrimination in the green-backed firecrown hummingbird (*Sephanoides sephaniodes*). *J. Comp. Physiol. A Neuroethol. Sens. Neural Behav. Physiol.* **194**, 785–794 (2008).
48. M. C. Stoddard *et al.*, Wild hummingbirds discriminate nonspectral colors. *Proc. Natl. Acad. Sci. U.S.A.* **117**, 15112–15122 (2020).
49. D. Osorio, M. Vorobyev, A review of the evolution of animal colour vision and visual communication signals. *Vision Res.* **48**, 2042–2051 (2008).
50. J. A. Endler, P. W. J. Mielke, Comparing entire colour patterns as birds see them. *Biol. J. Linn. Soc. Lond.* **86**, 405–431 (2005).
51. R. Maia, H. Gruson, J. A. Endler, T. E. White, pavo 2.0: New tools for the spectral and spatial analysis of colour in R. *Methods Ecol. Evol.* **10**, 1097–1107 (2018).